Title:
Molecular Mechanism of Condensin II auto-repression by NCAPD3 and activation by M18BP1

Authors:
Damla Tetiker[1,2]†, Kumiko Samejima[3] †, Yan Li[3], David Schaumann[1], David Barford[4], Luis Aragon[5], William C. Earnshaw[3], Erin E. Cutts[6,7]*, Eugene Kim[1]*, Kyle W. Muir[3]*
†These authors contributed equally to this work
*Corresponding authors. Email: e.cutts@sheffield.ac.uk, Eugene.Kim@biophys.mpg.de, kyle.muir@ed.ac.uk

[1]Max Planck Institute of Biophysics, 60438, Frankfurt am Main, Germany.
[2]IMPRS on Cellular Biophysics, Max-von-Laue-Straße 3, 60438, Frankfurt am Main, Germany.
[3]Institute of Cell Biology, University of Edinburgh, Edinburgh, UK.
[4]MRC Laboratory of Molecular Biology, Francis Crick Avenue, Cambridge, CB2 0QH, UK
[5]DNA Motors Group, MRC Laboratory of Medical Sciences (LMS), Du Cane Road, London, W12 0HS, UK.
[6]School of Biosciences, Faculty of Science, University of Sheffield, UK
[7]Nucleic Acid Institute, University of Sheffield, UK

Abstract:

Condensin is a conserved pentamer that reorganizes chromosomes in early mitosis. In this study we leverage single-molecule biophysics, cryo-electron microscopy (cryo-EM), and cell biology to dissect the molecular mechanism underlying condensin II auto-repression and activation. The C-terminal tail of NCAPD3 ($NCAPD3^{Tail}$) forms a belt around the N-terminus of the NCAPH2 subunit ($NCAPH2^{Neck}$) restraining its DNA-binding 'Neck' domain on the surface of the NCAPG2 subunit. Deletion of $NCAPD3^{Tail}$ causes spontaneous activation of condensin II *in vivo* and *in vitro*. Direct competition for the $NCAPD3^{Tail}$ binding site on NCAPG2 enables the condensin II activator M18BP1 to displace $NCAPD3^{Tail}$. This liberates $NCAPH2^{Neck}$ to form a DNA-binding interface together with NCAPD3/SMC2. In addition, M18BP1 forms a positively charged loop that wraps around NCAPG2 and stabilizes DNA-anchoring during loop extrusion. Together, these findings reveal a two-step activation mechanism in which M18BP1 relieves auto-repression and actively promotes stable DNA association during condensin II–mediated loop extrusion.

Main text:

During mitosis, chromosomes undergo a dramatic reorganization from their 'diffuse', physically entangled interphasic architecture into discrete resolved sister chromatids (*1, 2*) (*3*). The disentanglement process is fundamental to ensure that sister chromatids can be mechanically separated and evenly divided between daughter cells following the dissolution of sister-chromatid cohesion at the metaphase-to-anaphase transition(*4-6*). Mitotic chromosome assembly is largely driven by condensins which belong to the structural maintenance of chromosomes (SMC) family of DNA-binding ATPase motors(*7, 8*). A prevailing hypothesis is that condensins reshape chromatin through a combination of DNA loop extrusion, an ATP-dependent process in which condensin actively reels in DNA to enlarge loops, and DNA-bridging activities, whereby

condensin passively stabilizes physical contacts between distant DNA segments (*9-12*). Most eukaryotes, including humans, possess two condensin paralogues, condensin I, and condensin II(*8, 13*). Condensin I and II share the same SMC2/4 subunits but differ in the non-SMC subunits which are Kleisin (NCAPH and NCAPH2 for Condensin I and II respectively) and two HEAT-repeat HAWK subunits (NCAPG/D2 and NCAPG2/D3 for Condensin I and II respectively) (*8*). Architecturally, condensins are pentameric complexes, in which a single 'kleisin' protein, links together the two accessory HEAT-repeatHAWK proteins proteins around a heterodimeric SMC-ATPase core (*7*).

Condensin II, is less abundant than condensin I but is localized in the nucleus throughout the cell cycle and initiates chromosome condensation at mitotic entry (*1-3*). Following nuclear envelope breakdown, cytoplasmic condensin I gains access to chromosomes to form loops nested within larger condensin II loops (*1, 3, 14, 15*). During mitosis, condensin II co-operates with topoisomerase II alpha(*16*) to reorganize chromatin such that sister-chromatids can be resolved and segregated. Condensin II is an active ATPase(*17-19*) capable of binding and organizing DNA into loops *in vitro*(*20*), however the fundamental molecular mechanism by which this is achieved remains unclear.

Condensin activity is regulated by auto-repression, protein phosphorylation, and specific regulatory proteins, giving rise to differential control of condensin I/II. Current evidence suggests that condensin II is repressed and activated by the proteins MCPH1 and M18BP1, respectively. During interphase, depletion of MCPH1 leads to premature chromosome condensation (PCC) (*18, 21-26*). Interphase PCC induced by loss of MCPH1 can be suppressed by the co-depletion of M18BP1(*17*), implying the latter is required for condensin II activity(*27*). Regulator binding to condensin II is likely controlled by phosphorylation: CDK-1 mediated phosphorylation reduces MCPH1 repressor binding(*18*), but enhances M18BP1 activator binding, leading to a phospho-dependent switch toward activation during mitosis(*17*). Combined depletion of both MCPH1 and M18BP1 during interphase and mitosis results in loss of condensin II chromosome association(*17*), indicating condensin II is likely autoinhibited even in the presence of mitotic kinases. In *in vitro* chromosome reconstitution experiments, removal of the NCAPG2 subunit and the NCAPD3 C-terminal tail led to hypercondensed chromatin(*28, 29*), implicating these domains in autoinhibition. Although we now have a reasonable understanding of the regulatory factors, post-translational modifications, and autoinhibitory elements involved in controlling condensin II activation, how this is achieved at a mechanistic level remains an unsolved question.

Here, we employ a series of single-molecule, structural biochemistry and cell biological experiments to reveal the molecular basis of condensin II activation and activity during mitosis. This revealed an autoinhibitory mechanism in which the NCAPD3^{Tail} sequesters the NCAPH2^{Neck}, that is overcome during activation by release by the activator M18BP1. M18BP1 moreover not only activates condensin II but also contributes biochemically to stable loop extrusion.

Results

Structure of apo condensin II.

To investigate the molecular structure of condensin II, we first determined the structure of the apo complex, in the absence of ATP and DNA, using cryo-electron microscopy (cryo-EM). We observed both apo condensin II monomers and dimers (Fig. 1A). The dimeric population was more abundant on cryo-EM grids, and was thus the focus of higher-resolution structure determination, yielding an overall resolution of 3.6 Å (Fig. S1., Fig. S2A-F). This resolution was sufficient to unambiguously fit AlphaFold3 (*30*) predictions to the map, which were then manually adjusted.

The subpopulation of monomers in the dataset enabled assignment of the dimerization interface (Fig. 1A, Fig. S1B). As the overall configuration of each protomer appeared effectively similar (Fig. 1A), for further analysis we performed particle-symmetry expansion. To establish the architecture of the condensin II protomer monomer, we applied focused classification and local refinement approaches to determine a reconstruction at a resolution of 3.6 Å (Fig.1B., Fig. S1B,C, Fig. S2A-F).

We first focused on the dimerization interface, determining a local resolution of 3.9 Å (Fig. S1D). The condensin II complex forms a closed dimer mediated through contacts between the NCAPG2 subunit of one protomer and the C-terminus of the SMC4 subunit of the other (Fig. 1C). Recent studies have implicated this region of NCAPG2 in binding both MCPH1 and M18BP1 (*17, 18*). We also observed modest inter-protomer interactions between NCAPH2 subunits (Fig. S2A). Mutagenesis of this NCAPH2 region leads to poor chromosome axis formation *in vitro* (*28*).

We then analyzed the organization of the catalytic centre of the condensin complex: the SMC2/4 ATPase domains (Fig. 1B). SMC family proteins comprise globular N and C-terminal domains that fold together to generate a single ATPase, that is intersected by an extended stretch of antiparallel coiled-coil featuring a heterodimerization, or hinge, domain.

The SMC4 ATPase domain is well defined, whereas tSMC2 is considerably more mobile and is only resolved at the domain level in the monomer reconstruction (Fig. 1 A). In this moderate resolution reconstruction, the heads are not engaged in an ATP-binding competent configuration but rather are splayed apart (Fig. 1B, Fig. S3B). We observed clear classes for the coiled-coil including the SMC2/4 hinge heterodimerization domain (Fig. S1A,B) however its continuity with respect to the ATPase domains was unclear, indicating flexible linkage.

The kleisin subunit, NCAPH2, forms extensive contacts with the HEAT repeat subunits and binds SMC4 through its C-terminal winged-helix domain. NCAPH2 residues 146-197, 314-371, and 489-593 engage NCAPD3, NCAPG2 and SMC4, respectively (Fig. S3C). The region of NCAPH2 immediately emerging from the winged-helix domain (WHD) forms an additional contact with NCAPD3 via residues 466-483 within the monomer (Fig. S3D), whereas NCAPH2 residues 342-351 emerge from the surface of NCAPG2 to dock against the SMC4-NCAPH2 subcomplex of the adjacent protomer (Fig. S3A).

The HEAT-repeat proteins, NCAPG2 and NCAPD3, dock against one another using an **α**-helical 'docker' domain (*29*) (Fig. 1A,B; Fig. S3E), whereas the major SMC-HEAT contact within the

protomer monomer involves binding of NCAPD3 to the surface of SMC4, including its W-loop(*31, 32*) (Fig. 1B,D).

We observed map density on the surface of NCAPG2 subunit that could not be accounted for by NCAPG2 itself. Through further focused classification, we obtained maps enabling automated model-building of this region. This approach revealed that the additional density corresponds to the NCAPH2^{Neck}, spanning residues 24-95 (Fig. 1E, Fig. S1C). In related eukaryotic SMCs, the kleisin^{Neck} typically binds the coiled-coil of its cognate SMC, in this case SMC2, to form Neck 'gates' that regulate DNA entry or exit(*32-34*) (*35*). The presence of NCAPH2^{Neck} on NCAPG2 indicates that apo condensin II possesses an 'open' SMC2^{Neck}:NCAPH2^{Neck} gate.

We observed additional density directly bridging the NCAPH2^{Neck} and NCAPG2, deriving from the C-terminal NCAPD3^{Tail}, comprising amino-acids1454-1476 (Fig. 1E, Fig. S3C). Previously, it had been reported that *in vitro* deletion of 200 residues the NCAPD3 C-terminal tail (NCAPD3^{tail}) correlated with complex activation, whereas alanine substitution of NCAPD3^{tail} phosphorylation sites resulted in decreased activity(*28*). Indeed, S1458 and S1474, which are buried at the NCAPH2 and NCAPG2 binding interface, respectively, are phosphorylated in cells(*36-38*) and would be incompatible with NCAPD3^{Tail} binding (Fig. 1E).

We therefore hypothesize that the apo structure represents a nucleotide free form of condensin II, and that NCAPH2^{Neck} sequestration on the surface of NCAPG2 by the NCAPD3^{Tail} provides a potential mechanism to regulate condensin II activity.

Loop extrusion by monomeric condensin II complexes

Modelling ATP-dependent head engagement indicates a clash between the SMC2 and NCAPD3, which, due to the docking of NCAPG2 and NCAPD3, suggest dimer formation is incompatible with head engagement (Fig. S3B, F). Using mass photometry, we observed that even in the presence of low micromolar concentrations of ATP, the dimer fraction of condensin II effectively dissolves (Fig. 1F, Fig. S2G). To characterize the DNA organizing activity of condensin II *in vitro,* we employed a single-molecule assay that allows direct visualization of DNA topology and Alexa Fluor 647 labelled condensin II complexes. In this setup, linear 44.2 kilobase pair DNA molecules were tethered at both ends to a glass surface, stained with Sytox Orange (SxO) intercalating dye, and imaged with highly-inclined and laminated optical sheet microscopy (Fig. 1G). Upon introduction of ATP and single fluorophore labeled condensin II, we observed that condensin II bound to DNA and subsequently formed loops that gradually increased in size over time, indicative of active loop extrusion (Fig. 1G, H).

To determine stoichiometry of loop-extruding complexes, we analysed photobleaching steps during key events including DNA-binding and loop-extrusion (Fig. 1H). In the majority of cases, condensin II bound to DNA in a single step, followed by loop growth, and finally bleached in a single step (Fig. 1I). This indicates that the loop-extruding form of condensin II acts as a monomer, consistent with condensin I, and prior observations(*20, 39*). Furthermore, stoichiometric analysis of DNA-bound but non-loop-extruding complexes showed that most condensin II complexes were also monomeric (Fig. 1J).

Together, these results demonstrate that the DNA-binding and loop-extruding forms of condensin II are predominantly monomeric.

ATP-engaged auto-inhibited state

To understand how condensin II structurally reorganizes to accommodate nucleotide binding, we determined its structure in complex with ATP to a resolution of 3.8 Å (Fig. 2A, Fig. S2G,H,Fig. S4 A,B). The resulting complex is monomeric, in agreement with our in-solution measurements (Fig. 1F, Fig. S2G). The ATPase itself adopts a conformation similar to related SMC complexes, and the presence of ATP in the active site is clearly defined in the cryo-EM map (Fig. 2C,D). In this conformation, the structure of the HEAT-repeat subunit heterodimer is identical, however NCAPG2 replaces NCAPD3 to bind the SMC2/4 ATPase module (Fig. S4C). NCAPG2 forms extensive contacts with the surface of the SMC2 ATPase domain, and additionally binds through its N-terminus to the coiled-coils of SMC4 (Fig. 2B).

In this structure, the NCAPH2^{Neck} remains bound to NCAPG2, but further details of the NCAPD3 tail are apparent. Similar to the apo structure, NCAPD3^{Tail} residues 1454-1460 bind the NCAPH2^{Neck} whereas NCAPD3^{Tail} residues 1469-1476 bind NCAPG2. However, in the ATP-bound structure, we observe preceding residues 1336-1371 of NCAPD3^{Tail} bound to NCAPG2. By consequence, the NCAPD3^{Tail} effectively forms a proteinaceous belt that encloses NCAPH2^{Neck} domain on the surface of NCAPG2 (Fig. 2B).

Due to swapping of the HEAT repeat domains relative to the ATPase, the NCAPH2^{Neck} is repositioned in close vicinity to SMC2 (Fig. 2B, Fig. S4C). As a consequence, the NCAPH2^{Neck} now directly bridges NCAPG2 with the SMC2^{Neck} coils, but nevertheless remains sequestered by the NCAPD3^{Tail}.

Condensin II is auto-inhibited *in vivo*

Deletion of the NCAPD3^{Tail} activates condensin II *in vitro*(*28*), but this has not been investigated *in vivo.* To investigate the possibility that the NCAPD3^{Tail} impinges upon condensin II activity in cells, we implemented an assay to monitor chromosome morphology in DT40 cells arrested at the G2/M transition, prior to global chromatin compaction by condensin II, via inhibition of analogue-sensitive CDK1 (*1*). In this assay, we transiently express NCAPD3 protein (wild-type or mutants) in chicken DT40 CDK1^{as}/NCAPD3-AID cells and acutely depleted endogenous chicken NCAPD3 protein (gNCAPD3) by addition of 5-Ph-IAA(*40*) (Fig. S4D). The cells expressing wild-type gNCAPD3 exhibited chromosome morphologies equivalent to the wild type cells during G2 and also in mitosis. In contrast, the cells expressing gNCAPD3 with tail residues 1293-1493 deleted (gNCAPD3$^{\Delta Tail}$) and residues 1458-63 deleted (gNCAPD3$^{\Delta Tail\text{-}G2}$) underwent premature chromosome condensation (PCC) in G2 blocked cells (Fig. 2E, F and Fig. S2E).

Condensin II is repressed by MCPH1 and requires M18BP1 to condense chromatin (*17, 18, 24-27*). Similar to humans, MCPH1 and M18BP1 are both expressed in DT40 cells. In order to further dissect how these factors contribute to condensin II, we co-transfected cells with a plasmid encoding both guide RNAs (gRNAs) and Cas9 nuclease to inactivate the corresponding genes.

Two days after transfection with MCPH1 gRNAs, the majority of both wild-type and gNCAPD3$^{\Delta Tail}$ transfected cells underwent PCC at G2 phase (Fig. 2F). In case of M18BP1

gRNAs, no PCC was observed in both wild-type and gNCAPD3$^{\Delta Tail}$ transfected cells (Fig. 2F, G). When both guide RNAs for M18BP1 and MCPH1 are transfected, we observed marked differences in the phenotype between the wild-type and gNCAPD3$^{\Delta Tail}$ rescue conditions (Fig. 2G). Whereas MCPH1-mediated PCC was highly dependent on the M18BP1activator in the wild-type rescue, the gNCAPD3$^{\Delta Tail}$ expressing cells exhibited PCC even in the absence of the M18BP1 activator (Fig. 2G). A more subtle mutant removing the NCAPD3$^{Tail\text{-}G2}$ (gNCAPD3 residues 1458-1363; see Fig. 2B: NCAPD3$^{Tail\text{-}H2}$ interaction) showed an intermediate phenotype (Fig. 2E). From this set of experiments, we conclude that in DT40 cells, MCPH1 and M18BP1 perform an inhibitor/activator function comparable to their human equivalents, and moreover that condensin II is able to spontaneously compact chromatin independently of M18BP1 when the gNCAPD3^{Tail} is deleted (Fig. 2G). This suggests that the gNCAPD3^{Tail} imposes an intrinsic auto-inhibitory constraint on condensin II activity *in vivo*. We therefore hypothesized that this auto-inhibition reflects regulation of condensin II loop-extrusion activity and sought to test this directly *in vitro*.

Loop extrusion by condensin II is auto-inhibited by NCAPD3-tail and H2 neck interactions

We employed a single-molecule loop extrusion assay to test our structure-based hypothesis that sequestration of the NCAPH2^{Neck} by NCAPD3^{Tail} serves an autoinhibitory function. Loop-extrusion activity was quantified as looping probability, defined by the fraction of DNA molecules that formed at least one loop during a 1000-second acquisition period.

To dissect the proposed NCAPG2– NCAPH2^{Neck} – NCAPD3^{Tail} interaction, we generated a series of mutations predicted to disrupt this interface. Specifically, we deleted the entire NCAPG2 (ΔG2) and NCAPD3 (ΔD3) subunits, removed the final 200 amino acid residues of NCAPD3 that comprise the NCAPD3^{Tail} (NCAPD3$^{\Delta Tail}$), deleted six well-conserved amino-acid residues that mediate the interaction with NCAPG2 (NCAPD3$^{\Delta Tail\text{-}G2}$, see Fig.1E, Fig. 2B: NCAPD3$^{Tail\text{-}G2}$ interaction), introduced alanine substitutions at residues 1453-1458, inclusive, on NCAPD3 that form the H2–neck binding interface (D3$^{Tail\text{-}H2ala}$, see Fig. 1E, Fig. 2B: NCAPD3$^{Tail\text{-}H2}$ interaction).

All mutants exhibited stimulated ATPase activity (Fig. 2H, Fig. S4F, G), while all NCAPD3^{Tail} mutants resulted in an increase in loop extrusion activity relative to WT condensin II (Fig. 2I), with the most prominent enhancement observed for the NCAPD3$^{\Delta Tail}$. Fig. S4
These findings support our hypothesis that the sequestration of NCAPH2^{Neck} by the NCAPD3^{Tail} serves an auto-inhibitory function, and that the disruption of this interaction promotes loop extrusion activity of condensin II.

M18BP1 increases the loop extrusion activity of condensin II by releasing the NCAPD3^{Tail}

Recruitment of condensin II to chromosomes in mitosis requires binding of M18BP1 to the NCAPG2 subunit. Overlaying AlphaFold3(*30*) predictions of M18BP1 and NCAPG2 with our experimental structure of auto-inhibited condensin II shows clear overlap between the NCAPD3^{Tail} residues 1470-1475 and amino acids 1073-1078 of M18BP1 (Fig. S5A-C), suggesting that M18BP1 may activate condensin II by displacing the NCAPD3^{Tail} , and, consequently the NCAPH2^{Neck}. Truncation of NCAPD3 tail residues 1470–1475 results in increased loop-extrusion activity (Fig. 2I) and PCC *in vivo* (Fig. 2E,G), providing further support for an activation mechanism involving displacement of NCAPD3^{Tail}.

To investigate whether M18BP1 converts condensin II into an active form *in vitro*, we added M18BP1 at various molar ratios (1× to 100× excess) to 2 nM condensin II and monitored its effects on condensin II–mediated loop extrusion. Analysis of looping probability across different molar ratios (Fig. S5D) revealed that M18BP1 alone increases loop extrusion activity only moderately, even at high molar excess (Fig. 3A). Phosphorylation is required for robust M18BP1 binding to condensin II, hence we introduced CDK1/Cyclin B to our single-molecule assay. Condensin II and M18BP1 (2 nM and 50 nM, respectively) were pre-incubated with CDK1/Cyclin B (5 nM and 10 nM, respectively) prior to imaging. Under these conditions, we observed a marked stimulation of looping activity, with nearly all DNA molecules being organized into loops (Fig. 3A). This hyperactivation was completely eliminated by point mutations that specifically target the ability of M18BP1 to bind the NCAPD3^{Tail} overlapping region on NCAPG2 (M18BP1$^{D3\ mutant}$), without abolishing its general recruitment to condensin II (Fig. 3A, Fig. S5A-G).

To confirm that the enhanced looping activity arises from M18BP1–condensin II association, we co-localized condensin II-mediated loops with Janelia Fluor 646-labeled M18BP1 using a lower molar ratio (1:5). In the absence of CDK1/Cyclin B approximately 30 percent of DNA loops initiated at sites co-localized with an M18BP1 signal (Fig. S6A-B). At this concentration, M18BP1 alone showed minimal DNA binding (Fig. S6D-F), and M18BP1 binding to loops depended on the presence of condensin II containing NCAPG2 (Fig. S6A-C), indicating that loop formation resulted from specific association of M18BP1 with condensin II.

In agreement with looping probability measurements, pre-incubation of condensin II and labeled M18BP1 (2 nM and 10 nM, respectively) with CDK1/Cyclin B resulted in a two-fold increase in co-localization of M18BP1 at loop initiation sites, reaching 60 percent (n = 35) (Fig. 3B; Fig. S6A). This suggests that enhanced looping activity arises from increased M18BP1–condensin II binding affinity mediated by CDK1/Cyclin B.

Previous work suggests that phosphorylation of both NCAPD3 and M18BP1 contribute to activation. To further dissect the effect of CDK-dependent phosphorylation, we generated a set of samples where either condensin II (WT^{phos}) or M18BP1 alone (M18BP1^{phos}) or both together (WT^{phos}+M18BP1^{phos}) were phosphorylated with CDK1. Our experimental structure suggests phosphorylation would promote NCAPD3^{Tail} release by a combination of steric hindrance and charge repulsion at its interfaces with NCAPG2-NCAPH2^{Neck} (Fig. 1E). In contrast, phosphorylation of M18BP1 increases its binding affinity for condensin II(*17*). These effects may also be cooperative: M18BP1 binding could promote phosphorylation of NCAPD3^{Tail} by facilitating its release, or phosphorylation of NCAPD3^{Tail} could, in turn, assist efficient binding of M18BP1 to condensin II. Consistent with these hypotheses, we detected more NCAPD3^{Tail} phospho-peptides by mass spectrometry when M18BP1 was included together with CDK1 (Fig. S7A). Mass photometry further indicates that phosphorylation of either condensin II or M18BP1 increases their binding affinity, with the most pronounced effect observed upon M18BP1 phosphorylation (Fig. 3D).

The subsequent looping probability analysis revealed that phosphorylation of M18BP1 alone is sufficient to stimulate loop extrusion to a level comparable to the doubly phosphorylated sample (Fig. 3D). In contrast, phosphorylation of condensin II alone resulted in only a mild increase in looping activity, similar to unphosphorylated condensin II supplemented with M18BP1 (Fig. 3D). Together, these data indicate that M18BP1 phosphorylation plays the major role in activating

condensin II, presumably by enhancing its binding affinity to the complex, enabling it to displace NCAPD3^{Tail}.

M18BP1 releases the NCAPH2^{Neck} and reorganizes condensin II into a state 'poised' for DNA capture

To understand the molecular mechanism underlying activation of condensin II by M18BP1, we purified condensin II in complex with M18BP1, phosphorylated the complex with CDK1/cyclin B, and determined its structure in the presence of ATP (Fig. 3E, F, Fig. S7B, C). We observed both ATP-engaged and non-engaged forms of the SMC2/4 ATPases, to a resolution of 4.4 Å and 4.5 Å (Fig. S2I-N), respectively, and the HEAT repeat proteins again reoriented relative to the ATPase domains (Fig. S7D). Consistent with our prediction and single-molecule experiments, NCAPD3^{Tail} is displaced by M18BP1, which forms a highly extended interface with NCAPG2 (Fig. 3G, lower inset), including a 'localization' motif identified previously(*17*), resulting in release of the NCAPH2^{Neck} domain from NCAPG2 (Fig. 3G, upper inset). The NCAPH2^{Neck}, now disengaged from NCAPG2, is wedged between the C-terminal alpha-helices of NCAPD3 (Fig. 3H) and remains partially folded along the coiled-coils of the SMC2, in a conformation similar to the auto-inhibited state, with two key distinctions. Firstly, an **α**-helix comprising residues 13-24 of NCAPH2^{Neck} is displaced to accommodate slightly altered binding to the coiled-coils of SMC2, and secondly, the NCAPD3^{Tail} beta-strand that interacts with NCAPH2^{Neck} in the auto-inhibited state is now absent (Fig. 3H), potentially as a result of incompatible phosphorylation of NCAPD3^{Tail} residue S1458 (Fig. S7A).

In this structure, the reorganization of the HEATs positions the NCAPD3 positioned in close proximity to the coiled-coils of SMC2^{Neck}. In related eukaryotic SMCs, domains equivalent to SMC2^{Neck}:NCAPH2^{Neck} gate cooperates with the cognate HEAT, in this case NCAPD3, to form an ATP-dependent DNA-binding clamp(*33, 41-43*). Mapping of surface electrostatics showed that the NCAPD3 presents a positively charged surface to solvent in close proximity to the SMC2^{Neck}:NCAPH2^{Neck} gate (Fig. SE). We therefore anticipated that condensin II might also interface with DNA by assembling a structurally analogous 'clamp'.

Condensin II forms a DNA-binding clamp

To understand how condensin II reorganizes to bind DNA, we initially attempted to obtain a structure of condensin II bound to M18BP1 in the presence of DNA and phosphorylation, however the number of intact particles was limiting (Fig. S8A,B). By contrast, complexes of CDK1/CYCB phosphorylated condensin II assembled together with DNA yielded a cryo-EM reconstruction of the DNA-bound state to an overall resolution of 3.8 Å (Fig. S2O,P;Fig. S8C,D; Fig. 4A,B).

In this structure, DNA is 'clamped' between a composite interface formed by the ATP-engaged SMC2/4 heads, the now 'closed' neck (comprising NCAPH2^{Neck} and the coiled coils of SMC2), and sealed above by the NCAPD3-HEAT repeat (Fig. 4A,B). The SMC2^{Neck} coils (form a triple α-helical bundle with NCAPH2^{Neck} residues 53-85. The extended α-helix from NCAPH2^{Neck} results from refolding of the kleisin around a fulcrum (Fig. 4B, Fig. S8E). In the compact NCAPH2^{Neck} structures (apo, ATP-engaged, activated complexes), the N-terminal ~60 residues preceding this fulcrum fold to structurally mimic the SMC2^{Coils} (Fig. S8F).

The N-terminal region of NCAPD3 forms extensive contacts with and above the neck interface, crosses the face of the ATPases, and also directly bridges the coiled-coils of SMC2 and SMC4 immediately emerging from the ATPases (Fig. 4B). In this reconstruction, the NCAPG2 subunit is no longer visible, and we could not identify 2D classes corresponding to this subunit in the dataset. Instead, we observe that the **α**-helical docker domain that enables binding of NCAPD3 to NCAPG2 is now occupied by a contact with the SMC4 coiled-coils, indicating that separation of the HEAT repeat subunits is a consequence or requirement of clamped state assembly (Fig. S8G). Comparison of this structure with the limited 2D class averages, and low-resolution 3D reconstruction, recovered from the condensin II – M18BP1 – DNA complex (compare Fig. S8B, D) suggests that the overall organization of the central condensin II DNA clamp is structurally similar in the presence or absence of M18BP1 (Fig. S8A-D). This is consistent with our observation that NCAPG2, which is the only subunit within condensin II with which M18BP1 makes contact, is disengaged from NCAPD3 in the clamped state.

M18BP1 stabilizes condensin II–mediated loops by augmenting an NCAPG2-DNA anchor

To determine whether condensin II regulatory mechanisms influence loop dynamics, we analyzed loop kinetics for the different condensin II variants in single-molecule assays. The extrusion rate was not significantly different across samples (Fig. S9A). Wild-type condensin II functioned as a unidirectional loop extruder, consistent with the behavior of a single extruding complex, in which loop growth occurs as DNA is reeled in from one side of the complex (the motor side). DNA on the opposite, non-extruding side of the complex (the anchor side), however, frequently slipped out of the extruded loop, leading to increases in DNA length (Fig. 4C,D, Fig. S9B). This continuous DNA slippage resulted in rapid loop loss (Fig. 4C,D, Fig. S9B) and shorter loop lifetimes (Fig. 4G).

In the presence of M18BP1 and CDK1, condensin II formed markedly more stable loops, exhibiting extended stalling times (Fig. 4E,F, Fig. S9C) and increased loop lifetimes (Fig. 4G). This stabilization was primarily provided by improved anchoring of DNA, as evidenced by the DNA length remaining constant at the anchor side over extended periods (Fig. 4F, Fig. S9C). M18BP1-mediated loop stabilization was also observed with the M18BP1$^{D3\ mutant}$ and for the NCAPD3^{Tail} deletion mutant (NCAPD3$^{\Delta Tail}$) incubated with M18BP1, indicating that this effect is independent of NCAPD3^{Tail} displacement, suggesting that M18BP1 plays another functional role in addition to relieving autoinhibition of condensin II.
In our structure of M18BP1 – condensin II – ATP, we observed additional globular density bound to the NCAPG2 N-terminus (Fig. 4H, lower left inset). Modelling an AlphaFold3(*30*) prediction of NCAPG2-M18BP1 (Fig. S5B,C) into this density provided an unambiguous fit for the M18BP1 Myb domain (M18BP1^{Myb}, Fig. 4H, lower left inset). Connectivity of M18BP1^{Myb} to the remaining C-terminal regions of M18BP1 that decorate NCAPG2 is achieved by a ~40 amino-acid long linker that is rich in basic residues, in effect generating a positively charged loop (Fig. S10A-C). Previous studies have shown that the budding yeast NCAPG–kleisin chamber functions as a DNA-binding 'anchor' (*42, 44, 45*) that enables loop association during loop extrusion (*44*). We therefore hypothesized the M18BP1–NCAPG2 subcomplex may similarly act as a DNA anchor in condensin II. To test this hypothesis, we first performed electrophoretic mobility shift assays (EMSAs) to establish the DNA-binding properties of an NCAPG2-NCAPH2 subcomplex, and the modulation thereof by M18BP1. We observed that NCAPG2-H2 and M18BP1 individually shift DNA only weakly, indicative of low binding affinity (Fig. 4H, upper panel). In contrast, the NCAPG2-H2-M18BP1 trimer robustly shifts DNA. To test the role of the basic linker region in

M18BP1, we inserted charge-reversal mutations into residues K937E, K938E, K939E, K944E, K949E, R950E (M18BP1^{NC};Fig. S10B,C). We first established that the M18BP1 linker mutants do not measurably impact binding of M18BP1 to condensin II (Fig. S5F,G).

The charge-inversion mutations impaired DNA binding by M18BP1 alone and reduced its ability to augment DNA binding by the NCAPG2–NCAPH2 subcomplex (Fig. 4H, upper panel). Consistent with this defect, loop extrusion assays revealed that the basic loop mutations caused a significant reduction in condensin II–mediated loop extrusion activity to the level of WT condensin II alone (Fig. 4I).

Together, these results indicate that an additional DNA-binding site formed by M18BP1 and NCAPG2-NCAPH2 functions as a DNA anchor that stabilizes condensin II during loop extrusion, distinct from the structurally defined DNA-clamping site.

Discussion

In this study, we define a mechanistic framework for the auto-inhibition and activation of human condensin II (summarised in Fig. 4F). We show that condensin II is held in an inactive state through a mutually repressive architecture centered on the C-terminal tail of NCAPD3, which sequesters the NCAPH2 neck and prevents formation of an ATP-dependent DNA clamp. Activation proceeds through a two-step mechanism in which CDK1-dependent phosphorylation of M18BP1 enables binding of the activator M18BP1, leading to displacement of the NCAPD3^{Tail}, liberation of the NCAPH2^{Neck}, and reorganization of condensin II into a DNA-clamping–competent conformation. In addition to relieving auto-inhibition, M18BP1 contributes a composite DNA-binding interface together with NCAPG2–NCAPH2 that mechanically stabilizes loop extrusion. Together, these findings reveal how condensin II activity is both switched on and stabilized specifically during mitosis.

The kleisin domains of eukaryotic cohesins and condensins recruit two HAWK proteins, that regulate ATP-dependent DNA clamping (HAWK-A; NCAPD3$^{Condensin\ II\ A}$,NCAPD2$^{Condensin\ I\ A}$,PDS5/SCC2$^{cohesin\ A}$), and ATPase-independent DNA binding (HAWK-B: NCAPG2$^{Condensin\ II\ B}$,NCAPG$^{Condensin\ I\ A}$,SCC3$^{cohesin\ B}$). HAWK-B often has an additional role in providing a docking platform for regulatory factors that in turn can modulate SMC complex stability. In the presence of ATP, prior to condensin II activation, the clamping HAWK-A of condensin II, NCAPD3, is sterically occluded from the ATPase by HAWK-B, NCAPG2. This is achieved through a mutually repressive conformation in which the NCAPD3^{Tail} stabilizes binding of NCAPH2^{Neck} to NCAPG2, which in turn enables NCAPG2-NCAPH2^{Tail} to engage the ATPase of SMC2. This simultaneously prevents release of the polymorphic NCAPH2^{Neck} that partly refolds to participate in ATP-dependent DNA clamping (Fig.4B, Fig. S8E,F), and also creates a bridge between NCAPG2 and SMC2. Formation of this tripartite junction effectively blocks the DNA-binding site on the ATPase domain (Fig. S10D), and recruitment of the NCAPD3 DNA-binding domain to the neck gate. Our structural findings show that auto-inhibition therefore seems to resolve around sequestration of the NCAPH2^{Neck} by NCAPD3^{Tail}, and prevention of ATP-dependent DNA-clamp formation by NCAPD3.

Activation then must operate, at least partly, by overcoming NCAPD3^{Tail}, and indeed deletion of the repressive NCAPD3^{Tail} is sufficient to activate condensin II (Fig. 2. E-G; (*5, 29*)). Our study suggests auto-inhibition and activation of human condensin complexes have similar mechanistic features. In condensin I, the N-terminus of the kleisin is bound to NCAPG(*46*) and loss of this

region results in hyperactivity(*47*). Similarly, the C-terminal tail of NCAPD2 contributes to autoinhibition and competes with binding of activator KIF4A. As in condensin II, these interactions are primarily driven by extended disordered regions, which harbor multiple cell cycle specific phosphorylation sites (*46*).

Activation of condensin II is tightly coupled to mitotic entry through phosphorylation (*48, 49*). Cell cycle control of condensin II has long been attributed to phosphorylation, where early work demonstrated NCAPD3 is phosphorylated(*48*) and that loss of phosphorylation at T1415(*49*) impaired activity in human cells, while the activating condensin II in chicken cells(*50*). Phosphorylation, of NCAPH2 at S492 by Mps1(*51*), has also been implicated in activation. Previously it has been shown that CDK1 phosphorylation increases binding affinity of M18BP1 for condensin II (*17*). We propose CDK1 phosphorylation has a bipartite role in activation. Firstly, it enhances the capacity of M18BP1 activate condensin II, by releasing the NCAPH2^{Tail} through NCAPD3^{Tail} displacement. Furthermore, CDK1 phosphorylation of residues on NCAPD3^{Tail}, including interfacial phosphosites S1458 and S1474, could prevent NCAPD3 from rebinding NCAPH2^{Neck} and NCAPG2.

Beyond activation, our data reveal an unexpected role for M18BP1 in stabilizing condensin II–mediated loop extrusion. The budding yeast condensin I HAWK-B subcomplex features a 'safety-belt' in which the kleisin forms a proteinaceous loop anchoring condensin to DNA (*44, 45*).In contrast, we did not observe any such element within the kleisin of condensin II. Instead M18BP1 may add a DNA 'safety-belt' feature to the condensin II holocomplex to augment DNA binding and stabilize loop formation (*44*). Disruption of basic residues within the M18BP1 linker strongly impairs loop formation and stability without affecting complex assembly, demonstrating that M18BP1 actively promotes processive loop extrusion in addition to relieving autorepression.

More broadly, our findings emphasise the role of HAWK-B subunits (NCAPG2 for condensin II) at the center of condensin regulation. Across eukaryotic SMCs, HAWK-B is a focus of regulator recruitment (*17, 46, 52-56*) and can bind DNA independently (*42, 44, 45, 57-59*). Regulation of chromatin association of condensins(*17, 46, 52*) and cohesins(*17, 53-56*) via HAWK-B thus is emerging as a general mechanism for control of genome folding by eukaryotic SMCs

Condensin II is constitutively nuclear, yet only stably binds and globally compacts DNA during mitosis(*1, 2, 14, 18, 60, 61*), although it may have a role in maintaining interphase chromosome territories(*62, 63*). Premature activation of condensin II causes aberrant genome structure and pathology, including microcephaly(*18, 21-26*). Structurally, auto-inhibited condensin II is held in a configuration that is blocked from clamping DNA, and is kinetically suppressed through absence of a M18BP1 'safety-belt', that is pivotal for stable loop extrusion. Delegation of the 'safety-belt' to the extrinsic factor M18BP1, whose association with the complex can be regulated via several mechanisms, affords exquisite control over condensin II activation.

References:

1. J. H. Gibcus *et al.*, A pathway for mitotic chromosome formation. *Science* **359**, (2018).
2. K. Samejima *et al.*, Rules of engagement for condensins and cohesins guide mitotic chromosome formation. *Science* **388**, eadq1709 (2025).
3. N. Walther *et al.*, A quantitative map of human Condensins provides new insights into mitotic chromosome architecture. *J Cell Biol* **217**, 2309-2328 (2018).

4. A. M. O. Elbatsh *et al.*, Distinct Roles for Condensin's Two ATPase Sites in Chromosome Condensation. *Mol Cell* **76**, 724-737 e725 (2019).
5. E. M. Hildebrand *et al.*, Mitotic chromosomes are self-entangled and disentangle through a topoisomerase-II-dependent two-stage exit from mitosis. *Mol Cell* **84**, 1422-1441 e1414 (2024).
6. S. J. Klaasen, G. Kops, Chromosome Inequality: Causes and Consequences of Non-Random Segregation Errors in Mitosis and Meiosis. *Cells* **11**, (2022).
7. F. Burmann, J. Lowe, Structural biology of SMC complexes across the tree of life. *Curr Opin Struct Biol* **80**, 102598 (2023).
8. T. Hirano, Condensin-Based Chromosome Organization from Bacteria to Vertebrates. *Cell* **164**, 847-857 (2016).
9. T. Gerguri *et al.*, Comparison of loop extrusion and diffusion capture as mitotic chromosome formation pathways in fission yeast. *Nucleic Acids Res* **49**, 1294-1312 (2021).
10. M. Tang *et al.*, Establishment of dsDNA-dsDNA interactions by the condensin complex. *Mol Cell* **83**, 3787-3800 e3789 (2023).
11. S. Yatskevich, J. Rhodes, K. Nasmyth, Organization of Chromosomal DNA by SMC Complexes. *Annu Rev Genet* **53**, 445-482 (2019).
12. K. Kinoshita *et al.*, A loop extrusion-independent mechanism contributes to condensin I-mediated chromosome shaping. *J Cell Biol* **221**, (2022).
13. J. J. E. van Hooff, M. W. D. Raas, E. C. Tromer, L. Eme, Repeated duplications and losses shaped SMC complex evolution from archaeal ancestors to modern eukaryotes. *Cell Rep* **44**, 115855 (2025).
14. D. Gerlich, T. Hirota, B. Koch, J. M. Peters, J. Ellenberg, Condensin I stabilizes chromosomes mechanically through a dynamic interaction in live cells. *Curr Biol* **16**, 333-344 (2006).
15. N. Naumova *et al.*, Organization of the mitotic chromosome. *Science* **342**, 948-953 (2013).
16. K. Samejima *et al.*, Mitotic chromosomes are compacted laterally by KIF4 and condensin and axially by topoisomerase IIalpha. *J Cell Biol* **199**, 755-770 (2012).
17. A. Borsellini *et al.*, Condensin II activation by M18BP1. *Mol Cell* **85**, 2688-2700 e2611 (2025).
18. M. Houlard *et al.*, MCPH1 inhibits Condensin II during interphase by regulating its SMC2-Kleisin interface. *Elife* **10**, (2021).
19. P. Choppakatla *et al.*, Linker histone H1.8 inhibits chromatin binding of condensins and DNA topoisomerase II to tune chromosome length and individualization. *Elife* **10**, (2021).
20. M. Kong *et al.*, Human Condensin I and II Drive Extensive ATP-Dependent Compaction of Nucleosome-Bound DNA. *Mol Cell* **79**, 99-114 e119 (2020).
21. M. Arroyo *et al.*, Chromosome structure deficiencies in MCPH1 syndrome. *Chromosoma* **124**, 491-501 (2015).
22. H. Neitzel *et al.*, Premature chromosome condensation in humans associated with microcephaly and mental retardation: a novel autosomal recessive condition. *Am J Hum Genet* **70**, 1015-1022 (2002).
23. M. Trimborn *et al.*, Mutations in microcephalin cause aberrant regulation of chromosome condensation. *Am J Hum Genet* **75**, 261-266 (2004).

24. M. Trimborn, D. Schindler, H. Neitzel, T. Hirano, Misregulated chromosome condensation in MCPH1 primary microcephaly is mediated by condensin II. *Cell Cycle* **5**, 322-326 (2006).
25. J. L. Wood, Y. Liang, K. Li, J. Chen, Microcephalin/MCPH1 associates with the Condensin II complex to function in homologous recombination repair. *J Biol Chem* **283**, 29586-29592 (2008).
26. D. Yamashita *et al.*, MCPH1 regulates chromosome condensation and shaping as a composite modulator of condensin II. *J Cell Biol* **194**, 841-854 (2011).
27. J. M. Wenda, R. F. Prosee, C. Gabus, F. A. Steiner, Mitotic chromosome condensation requires phosphorylation of the centromeric protein KNL-2 in C. elegans. *J Cell Sci* **134**, (2021).
28. M. M. Yoshida *et al.*, Molecular dissection of condensin II-mediated chromosome assembly using in vitro assays. *Elife* **11**, (2022).
29. M. M. Yoshida, K. Kinoshita, K. Shintomi, Y. Aizawa, T. Hirano, Regulation of condensin II by self-suppression and release mechanisms. *Mol Biol Cell* **35**, ar21 (2024).
30. J. Abramson *et al.*, Accurate structure prediction of biomolecular interactions with AlphaFold 3. *Nature* **630**, 493-500 (2024).
31. B. G. Lee *et al.*, Cryo-EM structures of holo condensin reveal a subunit flip-flop mechanism. *Nat Struct Mol Biol* **27**, 743-751 (2020).
32. M. Hassler *et al.*, Structural Basis of an Asymmetric Condensin ATPase Cycle. *Mol Cell* **74**, 1175-1188 e1179 (2019).
33. T. L. Higashi *et al.*, A Structure-Based Mechanism for DNA Entry into the Cohesin Ring. *Mol Cell* **79**, 917-933 e919 (2020).
34. J. E. Collier, K. A. Nasmyth, DNA passes through cohesin's hinge as well as its Smc3-kleisin interface. *Elife* **11**, (2022).
35. M. Taschner, S. Gruber, DNA segment capture by Smc5/6 holocomplexes. *Nat Struct Mol Biol* **30**, 619-628 (2023).
36. A. N. Kettenbach *et al.*, Quantitative phosphoproteomics identifies substrates and functional modules of Aurora and Polo-like kinase activities in mitotic cells. *Sci Signal* **4**, rs5 (2011).
37. P. Mertins *et al.*, Integrated proteomic analysis of post-translational modifications by serial enrichment. *Nat Methods* **10**, 634-637 (2013).
38. K. Sharma *et al.*, Ultradeep human phosphoproteome reveals a distinct regulatory nature of Tyr and Ser/Thr-based signaling. *Cell Rep* **8**, 1583-1594 (2014).
39. M. Ganji *et al.*, Real-time imaging of DNA loop extrusion by condensin. *Science* **360**, 102-105 (2018).
40. A. Yesbolatova *et al.*, The auxin-inducible degron 2 technology provides sharp degradation control in yeast, mammalian cells, and mice. *Nat Commun* **11**, 5701 (2020).
41. J. E. Collier *et al.*, Transport of DNA within cohesin involves clamping on top of engaged heads by Scc2 and entrapment within the ring by Scc3. *Elife* **9**, (2020).
42. B. G. Lee, J. Rhodes, J. Lowe, Clamping of DNA shuts the condensin neck gate. *Proc Natl Acad Sci U S A* **119**, e2120006119 (2022).
43. Z. Shi, H. Gao, X. C. Bai, H. Yu, Cryo-EM structure of the human cohesin-NIPBL-DNA complex. *Science* **368**, 1454-1459 (2020).
44. I. A. Shaltiel *et al.*, A hold-and-feed mechanism drives directional DNA loop extrusion by condensin. *Science* **376**, 1087-1094 (2022).
45. M. Kschonsak *et al.*, Structural Basis for a Safety-Belt Mechanism That Anchors Condensin to Chromosomes. *Cell* **171**, 588-600 e524 (2017).

46. E. E. Cutts, D. Tetiker, E. Kim, L. Aragon, Molecular mechanism of condensin I activation by KIF4A. *EMBO J* **44**, 682-704 (2025).
47. S. Tane *et al.*, Cell cycle-specific loading of condensin I is regulated by the N-terminal tail of its kleisin subunit. *Elife* **11**, (2022).
48. T. Ono *et al.*, Differential contributions of condensin I and condensin II to mitotic chromosome architecture in vertebrate cells. *Cell* **115**, 109-121 (2003).
49. S. Abe *et al.*, The initial phase of chromosome condensation requires Cdk1-mediated phosphorylation of the CAP-D3 subunit of condensin II. *Genes Dev* **25**, 863-874 (2011).
50. M. Bakhrebah, T. Zhang, J. R. Mann, P. Kalitsis, D. F. Hudson, Disruption of a conserved CAP-D3 threonine alters condensin loading on mitotic chromosomes leading to chromosome hypercondensation. *J Biol Chem* **290**, 6156-6167 (2015).
51. Y. Kagami *et al.*, Mps1 phosphorylation of condensin II controls chromosome condensation at the onset of mitosis. *J Cell Biol* **205**, 781-790 (2014).
52. M. Wang *et al.*, Molecular mechanism targeting condensin for chromosome condensation. *EMBO J* **44**, 705-735 (2025).
53. X. Yuan *et al.*, Molecular mechanism and functional significance of Wapl interaction with the Cohesin complex. *Proc Natl Acad Sci U S A* **121**, e2405177121 (2024).
54. L. Yan *et al.*, A non-canonical role of the inner kinetochore in regulating sister-chromatid cohesion at centromeres. *EMBO J* **43**, 2424-2452 (2024).
55. A. Garcia-Nieto *et al.*, Structural basis of centromeric cohesion protection. *Nat Struct Mol Biol* **30**, 853-859 (2023).
56. Y. Li *et al.*, The structural basis for cohesin-CTCF-anchored loops. *Nature* **578**, 472-476 (2020).
57. Y. Li *et al.*, Structural basis for Scc3-dependent cohesin recruitment to chromatin. *Elife* **7**, (2018).
58. B. W. Bauer *et al.*, Cohesin mediates DNA loop extrusion by a "swing and clamp" mechanism. *Cell* **184**, 5448-5464 e5422 (2021).
59. K. Hara *et al.*, Structural basis of HEAT-kleisin interactions in the human condensin I subcomplex. *EMBO Rep* **20**, (2019).
60. T. Hirota, D. Gerlich, B. Koch, J. Ellenberg, J. M. Peters, Distinct functions of condensin I and II in mitotic chromosome assembly. *J Cell Sci* **117**, 6435-6445 (2004).
61. T. Ono, D. Yamashita, T. Hirano, Condensin II initiates sister chromatid resolution during S phase. *J Cell Biol* **200**, 429-441 (2013).
62. T. Ono *et al.*, Condensin II collaborates with cohesin to establish and maintain interphase chromosome territories. *J Cell Biol* **225**, (2026).
63. C. Hoencamp *et al.*, 3D genomics across the tree of life reveals condensin II as a determinant of architecture type. *Science* **372**, 984-989 (2021).
64. H. Ashkenazy *et al.*, ConSurf 2016: an improved methodology to estimate and visualize evolutionary conservation in macromolecules. *Nucleic Acids Res* **44**, W344-350 (2016).
65. Z. G. Zhang, J. Yang, D. Barford, Recombinant expression and reconstitution of multiprotein complexes by the USER cloning method in the insect cell-baculovirus expression system. *Methods* **95**, 13-25 (2016).
66. S. Yatskevich *et al.*, Structure of the human inner kinetochore bound to a centromeric CENP-A nucleosome. *Science* **376**, 844-852 (2022).
67. D. Kimanius, L. Dong, G. Sharov, T. Nakane, S. H. W. Scheres, New tools for automated cryo-EM single-particle analysis in RELION-4.0. *Biochem J* **478**, 4169-4185 (2021).
68. A. Rohou, N. Grigorieff, CTFFIND4: Fast and accurate defocus estimation from electron micrographs. *J Struct Biol* **192**, 216-221 (2015).

69. T. Wagner *et al.*, SPHIRE-crYOLO is a fast and accurate fully automated particle picker for cryo-EM. *Commun Biol* **2**, 218 (2019).
70. A. Punjani, J. L. Rubinstein, D. J. Fleet, M. A. Brubaker, cryoSPARC: algorithms for rapid unsupervised cryo-EM structure determination. *Nat Methods* **14**, 290-296 (2017).
71. P. Emsley, B. Lohkamp, W. G. Scott, K. Cowtan, Features and development of Coot. *Acta Crystallogr D Biol Crystallogr* **66**, 486-501 (2010).
72. P. V. Afonine *et al.*, Real-space refinement in PHENIX for cryo-EM and crystallography. *Acta Crystallogr D Struct Biol* **74**, 531-544 (2018).
73. E. C. Meng *et al.*, UCSF ChimeraX: Tools for structure building and analysis. *Protein Sci* **32**, e4792 (2023).
74. K. Jamali *et al.*, Automated model building and protein identification in cryo-EM maps. *Nature* **628**, 450-457 (2024).
75. F. Weissmann *et al.*, biGBac enables rapid gene assembly for the expression of large multisubunit protein complexes. *Proc Natl Acad Sci U S A* **113**, E2564-2569 (2016).
76. J. Yin, A. J. Lin, D. E. Golan, C. T. Walsh, Site-specific protein labeling by Sfp phosphopantetheinyl transferase. *Nat Protoc* **1**, 280-285 (2006).
77. M. Voulgaris, T. G. Gligoris, A Protocol for Assaying the ATPase Activity of Recombinant Cohesin Holocomplexes. *Methods Mol Biol* **2004**, 197-208 (2019).
78. L. C. Green *et al.*, Contrasting roles of condensin I and condensin II in mitotic chromosome formation. *J Cell Sci* **125**, 1591-1604 (2012).
79. B. Pradhan *et al.*, Loop-extrusion-mediated plasmid DNA cleavage by the bacterial SMC Wadjet complex. *Mol Cell* **85**, 107-116 e105 (2025).
80. J. Jumper *et al.*, Highly accurate protein structure prediction with AlphaFold. *Nature* **596**, 583-589 (2021).

Acknowledgements:
We acknowledge Diamond Light Source for access and support of the cryo-EM facilities at the UK's national Electron Bio-imaging Centre (eBIC) [under proposal EM BI31336], funded by the Wellcome Trust, MRC and BBRSC. This work was supported by funding for the Wellcome Discovery Research Platform for Hidden Cell Biology [226791] and we gratefully acknowledge support from the Proteomics and Structural Biology Cores. We thank the Vannini group (Human Technopole) for communicating unpublished results. We thank members of the Edinburgh chromosome supergroup for discussions. We thank Mohit Misra and Ivan Đikić for providing access to the mass photometry instrument. We thank Gabriele Maul for the preparation of biotinylated DNA.

Funding:
This work was funded by the Wellcome Trust (311085/Z/24/Z to KWM, and 107022/Z/15/Z to WCE), Sheffield University Physics of Life Fellowship (EEC), Medical Research Council UKRI MC-A652-5PY00 (LA) and MC_UP_1201/6 (DB), the Max Planck Society (EK), European Research Council Starting Grant 101076914 (EK) Deutsche Forschungsgemeinschaft (DFG, German Research Foundation)—SFB 1551 (DT and EK), and Cancer Research UK C576/A25675 (DB).

Author Contributions:

Conceptualization: E.C, E.K, K.W.M, K.S., D.T., Methodology: E.C, E.K, Y.L., K.W.M, K.S., D.T., Investigation: E.C, E.K, Y.L., K.W.M, D.S., K.S., D.T., Visualization: E.C,E.K, Y.L.,K.W.M, K.S.,D.T., Funding acquisition: L.A.,D.B.,E.C, W.C.E, E.K, K.W.M., Project administration: E.C., E.K., K.W.M., Writing – original draft: E.C, E.K, K.W.M, K.S., D.T., Writing – review & editing: E.C, W.C.E., E.K, K.W.M, Y. L., K.S., D.T.

Competing interests: The authors declare they have no competing interests.

Data, code, and materials availability:
Cryo-electron microscopy density maps were deposited with the Electron Microscopy Data Bank (EMDB), under accession codes:. Corresponding atomic coordinates were deposited with the Protein Data Bank (PDB), under accession codes:. All imaging data, cell lines and plasmids are available upon request to the corresponding authors.

Supplementary Materials

Materials and Methods
Figs. S1 to S10
Tables S1 to S2
References (*64–80*)

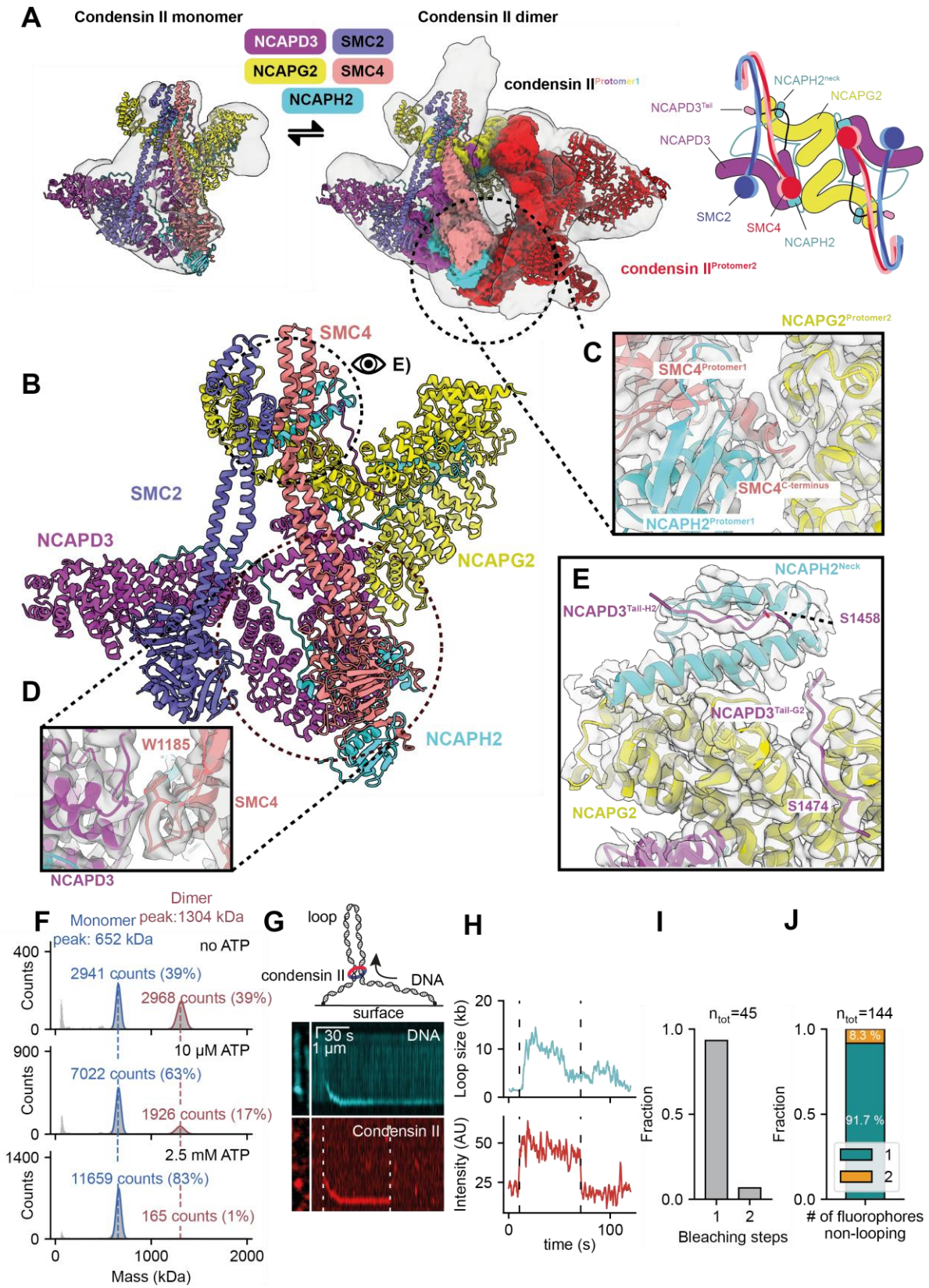
A
Condensin II monomer
Condensin II dimer
NCAPD3
SMC2
NCAPG2
SMC4
NCAPH2
condensin II Protomer1
condensin II Protomer2
NCAPH2 neck
NCAPD3 Tail
NCAPG2
NCAPD3
SMC2
SMC4
NCAPH2
B
SMC4
E)
SMC2
NCAPD3
NCAPG2
NCAPH2
C
NCAPG2 Protomer2
SMC4 Protomer1
SMC4 C-terminus
NCAPH2 Protomer1
D
W1185
SMC4
NCAPD3
E
NCAPH2 Neck
NCAPD3 Tail-H2
S1458
NCAPD3 Tail-G2
NCAPG2
S1474
F
Monomer peak: 652 kDa
Dimer peak:1304 kDa
no ATP
2941 counts (39%)
2968 counts (39%)
10 μM ATP
7022 counts (63%)
1926 counts (17%)
2.5 mM ATP
11659 counts (83%)
165 counts (1%)
Counts
Mass (kDa)
G
loop
condensin II
DNA
surface
30 s
1 μm
DNA
Condensin II
H
Loop size (kb)
Intensity (AU)
time (s)
I
n tot =45
Fraction
Bleaching steps
J
n tot =144
8.3 %
91.7 %
Fraction
# of fluorophores non-looping

Figure 1. Apo condensin II is in a monomer-dimer equilibrium and forms DNA loops as a monomer. (A) Cryo-EM 3D reconstructions of apo condensin II in a monomeric and dimeric state. Cartoon schematic of dimeric condensin II **(B)** Overall structural model of an apo condensin II protomer monomer. **(C)** Details of the dimerization interface of condensin II through the C-terminus of $SMC4^{Protomer\ 1}$ and $NCAPG2^{Protomer\ 2}$. **(D)** Cryo-EM density shows NCAPD3 contacts SMC4 through the W-loop of its ATPase domain. **(E)** The $NCAPD3^{Tail}$ interacts with NCAPG2 ($NCAPD3^{Tail\text{-}G2}$), and the $NCAPH2^{Neck}$ ($NCAPD3^{Tail\text{-}H2}$), sequestering it on the surface of NCAPG2. Potential phosphosites are highlighted. Cryo-EM density is displayed over the model to illustrate local map quality. **(F)** Histograms of condensin II mass distributions in the absence of ATP (top), in the presence of 10 μM ATP (middle) and in 2.5 mM ATP (bottom). **(G)** Representative snapshots and corresponding fluorescence intensity kymographs of a condensin II-mediated loop extrusion event, showing a SxO-stained DNA molecule (top) and Alexa 647-labeled condensin II (bottom). **(H)** Time traces of loop size (top) and condensin II fluorescence intensity (bottom) extracted from the loop extrusion event in **(G)**. **(I)** Fraction of loop-extruding condensin II molecules exhibiting either one- or two-step photobleaching. **(J)** Number of fluorophores per single binding event stoichiometry of DNA-bound non-loop-extruding condensin II molecules. $n_{tot} = 144$.

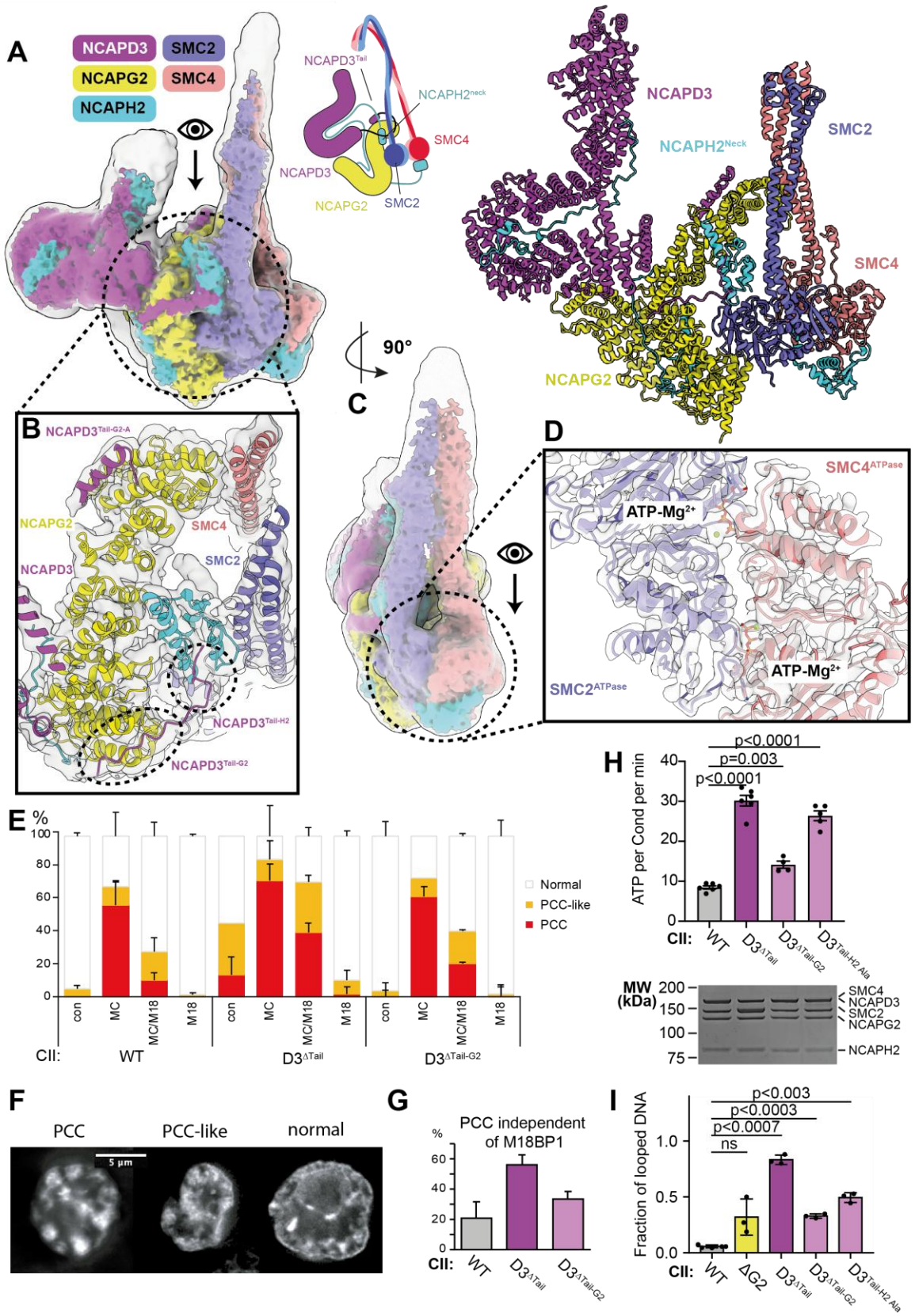
A
NCAPD3
SMC2
NCAPG2
SMC4
NCAPH2
NCAPD3Tail
NCAPH2neck
SMC4
NCAPD3
NCAPG2
SMC2
NCAPD3
NCAPH2Neck
SMC2
SMC4
NCAPG2
90°
C
B
NCAPD3Tail-G2-A
NCAPG2
SMC4
NCAPD3
SMC2
NCAPD3Tail-H2
NCAPD3Tail-G2
D
SMC4ATPase
ATP-Mg2+
ATP-Mg2+
SMC2ATPase
E
%
Normal
PCC-like
PCC
con
MC
MC/M18
M18
CII:
WT
D3ΔTail
D3ΔTail-G2
H
ATP per Cond per min
p<0.0001
p=0.003
p<0.0001
CII:
WT
D3ΔTail
D3ΔTail-G2
D3Tail-H2 Ala
MW (kDa)
SMC4
NCAPD3
SMC2
NCAPG2
NCAPH2
F
PCC
PCC-like
normal
5 µm
G
PCC independent of M18BP1
%
CII:
WT
D3ΔTail
D3ΔTail-G2
I
Fraction of looped DNA
p<0.003
p<0.0003
p<0.0007
ns
CII:
WT
ΔG2
D3ΔTail
D3ΔTail-G2
D3Tail-H2 Ala

Figure 2: ATP bound condensin II is inhibited via interactions of the C-terminal region of NCAPD3. (A) Consensus cryo-EM reconstruction of condensin II bound to ATP (left panel), and corresponding molecular model (right panel). A cartoon schematic of ATP-bound condensin II is shown **(B)** Zoomed-view of cryo-EM map density, showing the trajectory of NCAPD3^{Tail}. NCAPD3^{Tail} binds the N-terminus of NCAPG2 (NCAPD3$^{Tail\text{-}G2A}$), contacts the NCAPH2^{Neck} (NCAPD3$^{Tail\text{-}H2}$), and rebinds a second site on NCAPG2 (NCAPD3$^{Tail\text{-}G2}$), thereby forming a 'loop' around NCAPH2^{Neck}. **(C)** Front view of the condensin II – ATP complex. The consensus cryo-EM reconstruction is displayed as transluscent grey over a local-resolution filtered reconstruction coloured according to subunit. **(D)** Cryo-EM density contoured around the condensin II – ATP structure shows the presence of ATP and Mg^{2+} in the active site of the ATPase. **(E)** PCC assay of G2-arrested DT40 cells expressing wild-type (wt) or mutant GgCAPD3-mScarlet3. Chromosome morphology was classified as PCC, PCC-like, or normal. Guide RNAs targeted MCPH1 (M<u>C</u>), Mis18BP1/KNL2 (<u>M18</u>), or both (<u>MC/M18</u>). >50 mScarlet3-positive cells were scored per condition. Biological replicates: wt (n = 5), ΔC<u>ΔTail</u> (n = 4), 1458–1463 (n = 4). Mean + s.d. is shown. **(F) Ratio of PCC-positive cells in the absence of Mis18BP1/KNL2, calculated as PCC(<u>MC/M18</u>)/PCC(M<u>C</u>).** The difference between wt and ΔTail was significant (Kruskal–Wallis test). **(G)** Representative images of chromosome morphology in DT40 cells **(H)** ATP turn-over of condensin II WT, ΔG2, D3$^{\Delta TAIL}$, D3$^{\Delta 1470\text{-}1475}$ and D3$^{H2\ Alanine}$ mutants, error bars indicate mean and standard error. **(I)** Fractions of DNA molecules with condensin II-mediated loops in the presence of 2 nM condensin II and 2.5 mM ATP for WT, ΔG2, D3$^{\Delta Tail}$, D3$^{\Delta Tail\text{-}G2}$ and D3$^{Tail\text{-}H2\ Alanine}$ mutant. Mean ± s.d. is shown. n_{tot} = 704, 292, 477, 333, 403, respectively. Data are from at least three independent experiments. The P values were calculated using Welch's t test.

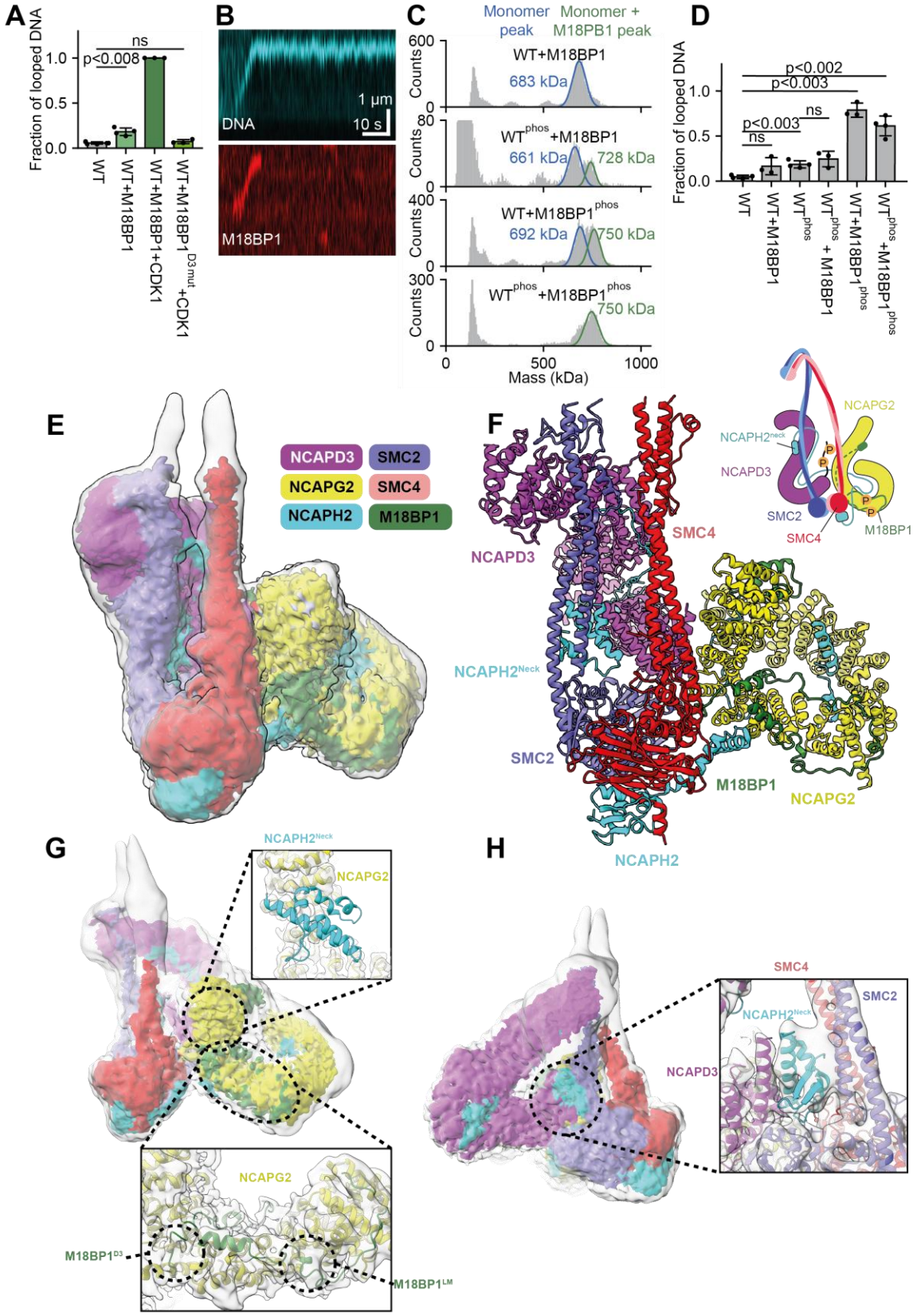
A
Fraction of looped DNA
ns
p<0.008
WT
WT+M18BP1
WT+M18BP1+CDK1
WT+M18BP1D3mut+CDK1
B
1 µm
10 s
DNA
M18BP1
C
Monomer peak
Monomer + M18PB1 peak
WT+M18BP1
683 kDa
WTphos+M18BP1
661 kDa
728 kDa
WT+M18BP1phos
692 kDa
750 kDa
WTphos+M18BP1phos
750 kDa
Counts
Mass (kDa)
D
Fraction of looped DNA
p<0.002
p<0.003
p<0.003
ns
ns
WT
WT+M18BP1
WTphos
WTphos + M18BP1
WT+M18BP1phos
WTphos+M18BP1phos
E
NCAPD3
SMC2
NCAPG2
SMC4
NCAPH2
M18BP1
F
NCAPD3
SMC4
NCAPH2Neck
SMC2
M18BP1
NCAPG2
NCAPH2
NCAPH2neck
NCAPD3
SMC2
SMC4
M18BP1
G
NCAPH2Neck
NCAPG2
NCAPG2
M18BP1D3
M18BP1LM
H
SMC4
SMC2
NCAPH2Neck
NCAPD3

Figure 3: M18BP1 activates condensin II by displacing NCAPD3^{Tail}, allowing condensin II DNA-clamp assembly. (A) Fractions of DNA molecules exhibiting condensin II-mediated loops in the presence of 2 nM condensin II and 2.5 mM ATP with either 200 nM M18BP1; 50 nM M18BP1 and 5 nM CDK1/10 nM CyclinB; or 50 nM M18BP1$^{D3\ mutant}$ and 5 nM CDK1/10 nM CyclinB. Mean ± s.d. is shown. n_{tot} = 704, 523, 348, and 310, respectively. Data are from at least three independent repetitions. The data for condensin II WT are reproduced from Fig. 2I. The P values were calculated using Welch's t test. **(B)** Representative kymographs of a looping event by M18BP1 bound-condensin II in the presence of CDK1/Cyclin B, showing a SxO-stained DNA molecule (top) and Janelia Fluor 646-labeled M18BP1 (bottom). **(C**) Histograms of mass distributions for the indicated samples: WT+M18BP1, WT_{phos}+M18BP1, WT+$M18BP1_{phos}$ and WT_{phos}+$M18BP1_{phos}$. Representative datasets from multiple independent experiments are shown. **(D**) Fractions of DNA molecules exhibiting condensin II-mediated loops in the presence of 2 nM condensin II and 2.5 mM ATP for WT, WT+M18BP1, WT_{phos}, WT_{phos}+M18BP1, WT+$M18BP1_{phos}$ and WT_{phos}+$M18BP1_{phos}$. Mean ± s.d. are shown. n_{tot} = 774, 533, 798, 374, 564, 754 respectively. Data are from at least three independent experiments. The P values were calculated using Welch's t test. **(E)** Consensus cryo-EM reconstruction of condensin II bound to ATP and M18BP1, and corresponding molecular model **(E)**. A cartoon schematic of ATP/M18BP1-bound condensin II is shown. (P) signifies phosphorylation. **(G)** Structure of CII bound to M18BP1 and ATP. Upper right inset shows cryo-EM map density contoured around NCAPG2. In the activated state, there is no map density for NCAPH2^{Tail} on NCAPG2, indicating it has been released. Lower right panel: cryo-EM density for M18BP1 indicates it binds multiple sites on NCAPG2, including a site overlapping with where NCAPD3^{Tail} binds in the inhibited state. **(H)** Rotated view of the M18MP1/ATP-bound CII structure. Inset panel shows cryo-EM map density contoured around NCAPH2^{Neck} which has relocated to the SMC2^{Neck} region.

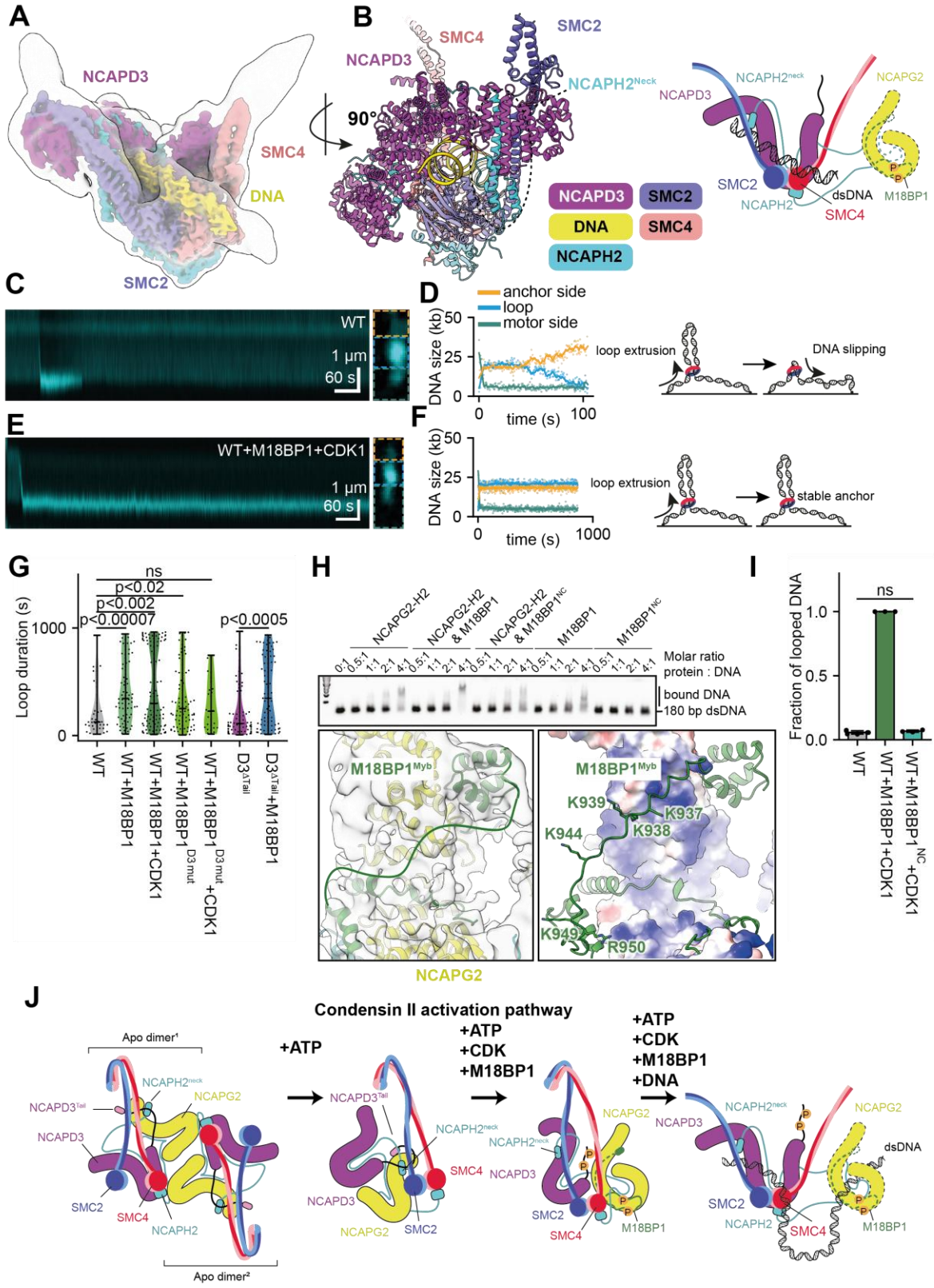
A
NCAPD3
SMC4
DNA
SMC2
B
SMC4
SMC2
NCAPD3
NCAPH2Neck
90°
NCAPD3
SMC2
DNA
SMC4
NCAPH2
NCAPH2neck
NCAPG2
NCAPD3
SMC2
NCAPH2
dsDNA
M18BP1
SMC4
C
WT
1 µm
60 s
D
anchor side
loop
motor side
DNA size (kb)
50
25
0
0
time (s)
100
loop extrusion
DNA slipping
E
WT+M18BP1+CDK1
1 µm
60 s
F
DNA size (kb)
50
25
0
0
time (s)
1000
loop extrusion
stable anchor
G
Loop duration (s)
1000
0
ns
p<0.02
p<0.002
p<0.00007
p<0.0005
WT
WT+M18BP1
WT+M18BP1+CDK1
WT+M18BP1D3 mut
WT+M18BP1D3 mut+CDK1
D3ΔTail
D3ΔTail+M18BP1
H
NCAPG2-H2
NCAPG2-H2 & M18BP1
NCAPG2-H2 & M18BP1NC
M18BP1
M18BP1NC
Molar ratio protein : DNA
0:1 0.5:1 1:1 2:1 4:1
bound DNA
180 bp dsDNA
M18BP1Myb
K939
K937
K938
K944
K949
R950
NCAPG2
I
Fraction of looped DNA
1.0
0.5
0.0
ns
WT
WT+M18BP1+CDK1
WT+M18BP1NC+CDK1
J
Condensin II activation pathway
Apo dimer1
NCAPH2neck
NCAPG2
NCAPD3Tail
NCAPD3
SMC2
SMC4
NCAPH2
Apo dimer2
+ATP
NCAPD3Tail
NCAPH2neck
SMC4
NCAPD3
NCAPG2
SMC2
+ATP
+CDK
+M18BP1
NCAPG2
NCAPH2neck
NCAPD3
SMC2
SMC4
M18BP1
+ATP
+CDK
+M18BP1
+DNA
NCAPH2neck
NCAPG2
NCAPD3
dsDNA
SMC2
NCAPH2
SMC4
M18BP1

Figure 4: M18BP1 stabilizes condensin II loops by providing a DNA anchor.
(A) Consensus cryo-EM reconstruction of the condensin II – ADP.BeFx – DNA complex. A local-resolution filtered reconstruction is colored according to subunit assignment. The SMC2/4 coiled coils are splayed apart compared to other structural states, and DNA is bound across a composite surface formed by the condensin II ATPase domains. A cartoon schematic is shown (P) signifies phosphorylation **(B)** Rotated view of local-resolution filtered map density for the condensin II – ADP.BeFx – DNA complex coloured according to subunit. DNA is topologically enclosed by formation of a clamp. The compartment is sealed from above by the NCAPD3 subunit that forms a tripartite DNA-binding interface with the $NCAPH2^{Neck}$:$SMC2^{Neck}$, and below by the SMC2/SMC4 ATPase domains. **(C, E)** Representative kymograph of a loop extrusion event by WT condensin II (C) and by condensin II in the presence of M18BP1 and Cyclin B/CDK1 (E), showing SxO-stained DNA molecules. **(D, F)** DNA lengths extracted from the corresponding kymographs in (C) and (E), respectively, for regions outside the loop (motor and anchor sides) and within the loop (Loop). **(G)** Loop duration times for loops formed by WT condensin II and in the presence of M18BP1; M18BP1 plus CDK1, $M18BP1^{D3\ mutant}$ and $M18BP1^{D3\ mutant}$ plus CDK1. n=41, 78, 106, 86, 29, respectively. The P values were calculated using Wilcoxon rank-sum test. **(H)** Electrophoretic mobility shift assay (EMSA) of an NCAPG2-NCAPH2 subcomplex in the presence or absence of indicated M18BP1 variants titrated against DNA (upper panel). Molar ratios and the position of unbound vs. shifted DNA are indicated. Data are from at least three independent replicates. A zoomed view of the NCAPG2-NCAPH2-M18BP1 subcomplex in the ATP/M18BP1-condensin II structure with cryo-EM map density displayed translucently shows separation of two M18BP1 regions connected by a flexible linker, drawn as a cartoon (lower left). Surface charge of NCAPG2 and positions of positively charged residues within an AlphaFold3(*30*) prediction of M18BP1 are displayed (lower right) **(I)** Fractions of DNA molecules exhibiting condensin II-mediated loops in the presence of 2 nM condensin II and 2.5 mM ATP with either 50 nM M18BP1 and 5 nM CDK1/10 nM CyclinB or 50 nM $M18BP1^{NC\ mutant}$ and 5 nM CDK1/10 nM CyclinB. Mean ± s.d. is shown. n_{tot} = 704, 348, and 390, respectively. Data are from at least three independent repetitions. The data for condensin II WT and condensin II WT + M18BP1 + CDK1 are are reproduced from Fig. 3A. The P values were calculated using Welch's t test.
(J) Cartoon schematic of condensin II activation. (P) signifies phosphorylation. Apo condensin II reorganizes into a monomer upon binding of ATP. Sequestration of $NCAPH2^{Neck}$ by $NCAPD3^{Tail}$ maintains auto-inhibition. Binding of M18BP1 to condensin II displaces $NCAPD3^{Tail}$, exposing it for phosphorylation. Displacement of the $NCAPD3^{Tail}$ releases $NCAPH2^{Neck}$, which is then able to participate in DNA clamp formation, and downstream DNA organization. DNA binding by the NCAPG2-NCAPH2-M18BP1 subcomplex stabilizes loop formation.